SSRG International Journal of Electrical and Electronics Engineering
ISSN: 2348-8379/ https://doi.org/10.14445/23488379/IJEEE-V11I3P113

Volume 11 Issue 3, 165-177, March 2024

Original Article

Smart Controllers Enabled Dynamic Energy Routing in DC-Grid PV Systems with Uninterrupted EV Charging

S.V. Kirubakaran[1], S. Singaravelu[2]

[1,2]*Department of Electrical Engineering, Annamalai University, Tamilnadu, India.*

[1]*Corresponding Author : evergreensr@gmail.com*

Received: 08 January 2024 Revised: 06 February 2024 Accepted: 07 March 2024 Published: 25 March 2024

Abstract - *Revealing a shift in energy management, this research introduces intelligent energy routing in a dynamic DC-grid integrated Photovoltaic (PV) system named Dynamic Energy Routing (DER). The system features a robust PV array, an enhanced DC-DC boost converter, and a Machine Learning-Support Vector Regression (ML-SVR) MPPT controller connected to a common DC grid. Complementing this setup is a standby battery with a 40AH capacity synchronized with an AC grid through a universal bridge rectifier controlled by an Artificial Neural Network (ANN). Integrating an Electric Vehicle (EV) charging station into the DC grid enhances the system's versatility. This research explores the dynamic behaviour of a DC-grid integrated PV system under varying State of Charge (SOC) conditions of the standby battery. In scenarios where the standby battery's SOC is high (≥70%), the system intelligently directs power from the PV system and standby battery to both the EV battery and the AC grid. This strategic routing is activated in response to adverse PV irradiance conditions by ensuring efficient energy utilization. In situations with moderate SOC levels (≤50%), the PV system and standby battery collaborate to supply power to the grid and EV batteries. However, the AC grid intervenes early to adapt to the moderate SOC and reduced irradiance conditions. In low standby battery SOC (<10%), the PV system takes charge by providing charging power to both the standby and EV batteries. In this scenario, the AC grid is promptly activated to contribute the necessary charging power by showing the system's adaptive response to diverse SOC levels and ensuring reliable energy distribution. Notably, the AC grid activation has done at worst irradiances and lower SOC of standby battery power. This research provides valuable insights into the system's adaptive and efficient energy routing strategies that contribute to understanding smart control mechanisms in DC-grid integrated PV systems with standby batteries and electric vehicle charging stations.*

Keywords - *ANN, ANFIS, ML-SVR, PV, Efficiency, SOC, EV, MPPT, DC grid.*

1. Introduction

In the next few years, a significant surge in global renewable electricity capacity is anticipated, with projections indicating a growth of over 60% compared to 2020 levels by 2026. This surge is expected to reach an impressive total of over 4,800 gigawatts to match the existing combined power capacity of fossil fuels and nuclear energy worldwide. Renewable energy sources are poised to play a pivotal role in this expansion, contributing to almost 95% of the overall increase in global power capacity from now until 2026 [1]. Among these renewable sources, solar PV technology is expected to emerge as a frontrunner by contributing more than half of the total growth. This forecast underscores a notable shift towards cleaner and more sustainable energy alternatives by signifying a significant withdrawal from traditional fossil fuels and nuclear power [1]. In the transition to a more environmentally conscious energy landscape, the global power sector is poised for a significant redefinition in the coming years by increasing renewables' dominance, especially solar PV [2].

Solar PV technology is fundamental in the global endeavour to shift towards more sustainable and environmentally friendly energy systems. This document delves into the crucial role of PV technology in mitigating greenhouse gas emissions and addressing the vital challenge of climate change. At the core of its effectiveness lies the performance of PV materials by governing the degree to which sunlight is converted into electrical power. Over the past decade, significant progress in PV efficiency has driven the widespread acceptance of solar PV technology worldwide [3]. The effectiveness of PV materials, particularly thin-film single junction Gallium Arsenide (GaAs) semiconductors, is a pivotal factor in determining how proficiently sunlight is converted into electrical energy. Considerable attention has been directed towards advancing thin-film solar cells due to their lightweight and flexible characteristics. Among these, the GaAs thin-film solar cell emerges as a leading entrant in the market because of its remarkable power conversion efficiency compared to other thin-film solar cell technologies [4].

The monocrystalline silicon (m-Si) thin-film solar cell underwent testing at the Sandia Test Centre in March 1999, which exhibits an efficiency of 25.0% with a tolerance of ±0.5%. On the other hand, the GaAs thin-film solar cell underwent testing at Atla Devices in the USA/New York by demonstrating an efficiency of 29.1% with a tolerance of ±0.6% [5].

Microgrids are environmentally sensible power systems harnessing renewable resources like solar and wind energy as their primary sources. However, the inherent unpredictability of wind and solar power poses a significant problem to the optimal functioning of microgrids [6].

The reliability of microgrid operations depends on the unpredictable nature of renewable energy harvesting. To overcome these challenges, microgrids incorporate energy storage systems such as batteries, flywheels, and supercapacitors to mitigate the impact of the intermittent nature of renewable energy sources. Acknowledging the complexity of environmental challenges such as climate change and natural resource degradation will underline the need for intelligent and innovative solutions [7].

There are several types of Maximum Power Point Tracking (MPPT) techniques were applied to increase energy harvesting including traditional (P&O, INC, FOCV, and HC) [8-11], intelligent (PI, and PID), AI (FLC, ANN, and ANFIS) [12-14] and recently ML techniques (linear regression, decision tree, random forest and naive bayes) [15].

To address challenges posed by dynamic and non-linear weather conditions impacting PV systems, the application of Machine Learning (ML) methods is promoted for optimizing energy generation. ML offers adaptability and predictive capabilities crucial for navigating the complexities associated with non-linear data, promising improved efficiency and effectiveness in diverse environmental scenarios [16].

The ML technique can effectively handle classification and regression tasks through recursive data partitioning, which holds promise for capturing the intricate and non-linear relationships within the PV system's data. DER in integrated systems refers to the capability of efficiently managing and distributing energy based on demand, availability, and system conditions.

Dynamic energy routing helps balance the fluctuations in supply and demand by intelligently routing energy to where it is needed most at any given time. Dynamically routing energy based on system conditions helps prevent overloads, reduce losses, and ensure a reliable power supply. The growing significance of standby batteries is attributed to their crucial role in providing backup power and ensuring uninterrupted operation under critical power requirements [17].

Standby batteries are a reliable backup power source during electrical outages or disruptions in the PV power supply. This is particularly critical for applications with continuous power, like EV charging centres, telecommunications infrastructure, hospitals and emergency response systems. The integration of DC grid systems encounters challenges such as voltage stability and control in DC grids, AC grid synchronization, integration of energy storage, dynamics in behaviour and transient stability analysis and implementation of advanced control techniques for power converters [18].

The widespread adoption of EVs has led to a growing need for a comprehensive charging infrastructure. As more EVs hit the roads, integrating EV charging stations has become crucial to urban planning and energy management. This integration has multifaceted implications for energy demand and distribution systems [19].

The interaction between EV charging stations and DC-grid integrated PV systems presents an opportunity to enhance sustainability. Solar energy generated by PV systems can be directly utilized for EV charging by reducing dependency on conventional grid power. Peak demand periods might experience a surge due to simultaneous charging activities, leading to the integration of the PV system with the AC grid to handle the additional load [20].

DC grid-integrated PV systems and EV charging stations create a localized and more resilient energy ecosystem. This reduces the reliance on centralized power generation and long-distance distribution by contributing to energy independence and minimizing transmission losses.

The authors Abraham D.S et al. present a grid-connected PV-powered EV charging station with a bidirectional converter, fuzzy logic control and a focus on decentralized power distribution and effective energy management. The authors considered the variability of PV power and different SOC levels in the energy storage unit under realistic scenarios, and the proposed system's effectiveness was validated through simulations and experiments [28].

The authors Alidrissi Y et al. were involved in developing and analysing a DC microgrid focusing on an energy management strategy. Their research includes the design of the microgrid, consideration of battery lifetime, simulation using Matlab/Simulink and validation of the proposed system's performance and stability under various operational scenarios [29]. The existing studies do not extensively explore the adaptive control mechanisms implemented in DC-grid integrated PV systems with standby batteries and electric vehicle charging stations. A research gap exists in understanding the nuances of smart energy routing and control strategies, particularly under varying State of Charge (SOC) conditions. A research gap exists in comprehending how the

system efficiently adapts and activates the AC grid in challenging situations to ensure reliable energy distribution. Previous research might not adequately address the integration challenges of incorporating EV charging stations into DC grids. The research gap lies in understanding how the system's versatility is affected by the addition of an EV charging station and how it dynamically allocates power resources in response to varying SOC levels. There is also a research gap in understanding the effectiveness and adaptability of the machine learning components in enhancing the system's overall performance.

The motivation of this work includes an efficient and dynamic energy routing to maximize the utilization of renewable energy generated by PV systems for EV charging. Optimizing energy flow from the solar panels to the charging stations involves developing smart (ML SVR) control strategies considering energy availability, demand patterns and storage capacity. The research seeks to minimize the environmental impact of EV charging by optimizing energy routing. By prioritizing using clean, renewable energy sources, reducing greenhouse gas emissions, and mitigating climate change, the research aims to develop a sustainable and resilient energy ecosystem that supports the widespread adoption of electric vehicles.

Identifying the need for dynamic energy routing strategies addresses the gaps and forms the basis for focused investigation. The intermittent and variable solar power generation in PV systems introduces uncertainties in energy availability. Identifying dynamic energy routing strategies is crucial to efficiently handle fluctuations in energy inputs and ensure reliable charging for EVs. EV charging demand is dynamic and influenced by various factors such as time of day, day of the week and special events.

Dynamic routing strategies are needed to align the energy supply with the dynamic charging demand, optimizing renewable energy and grid resource utilisation. ML-SVR-based smart MPPT control, ANN control for inverter and PI control for bidirectional DC-DC controller for battery storage have been implemented to optimize energy routing within the integrated system. These controllers were implemented by considering solar power generation, EV charging demand and energy storage capacity to make dynamic decisions for efficient energy routing. ML-SVR model can learn from historical data to make predictions and decisions that improve system efficiency and responsiveness to changing conditions.

This research addresses a critical problem in the need for sophisticated and adaptive energy routing strategies in DC-grid integrated PV systems. The problem lies in the absence of comprehensive studies investigating the particulars of smart energy routing by incorporating robust PV arrays, enhanced DC-DC boost converters and machine learning-based controllers. Furthermore, integrating an EV charging station into the DC grid increases the system's complexity by necessitating a nuanced understanding of how the system adapts and optimally distributes power in real-time. The problem statement encompasses the challenges of ensuring reliable energy distribution while maximizing energy utilisation efficiency, especially in situations where standby battery SOC levels vary widely. This research aims to bridge these gaps by investigating and proposing intelligent energy routing strategies that address the adaptive response of the system to diverse SOC conditions, adverse PV irradiance and the presence of an EV charging station. The study contributes to advancing DC-grid integrated PV systems and provides insights into the broader domain of smart control mechanisms in sustainable energy management.

The work is structured into four interconnected sections, each addressing specific aspects of the comprehensive system design and control strategies for a sustainable energy framework. Section one explains the design considerations for pivotal components such as the PV system, DC-DC boost converter, standby battery, EV battery and Universal Bridge Inverter (UBI). Detailed specifications and functionalities of each element provide a comprehensive foundation for the subsequent sections.

Section two explores the modelling of control strategies by highlighting the utilization of ANN and ML-SVR models. This section aims to provide insights into the workings of control mechanisms, explaining the parameters and structures employed for effective system regulation. Section three integrates all designed components and control strategies through the SIMULINK platform for simulation analysis. Finally, Section four serves as the conclusion by encapsulating a concise summary of findings, acknowledging limitations and proposing avenues for future research. The overall graphical outline of the proposed work is shown in Figure 1.

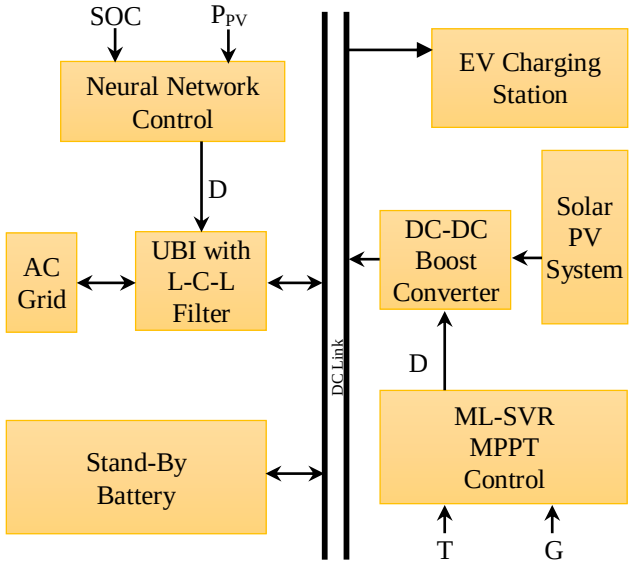

Fig. 1 Graphical outline of proposed system

2. System Components

2.1. Robust PV Array

When sunlight strikes a PV cell, it triggers the formation of electron-hole pairs as the cell's materials absorb photons with energy that exceeds the material's band gap. These generated carriers undergo separation due to the internal electric fields within the cell [21].

Connecting the cell to an external circuit allows these separated carriers to contribute to the overall current in a series of parallel connections. In recent years, significant research efforts have been dedicated to advancing thin-film solar cells because of the need for reduced weight and higher efficiency at variable temperature limits. Various structures of thin-film light-absorbing single junction semiconductor solar cells like Cadmium Telluride (CdTe), amorphous Silicon (a-Si), Copper Indium Di Selenide (CIS), and Gallium Arsenide (GaAs), have been explored [22].

The rivalry between silicon and gallium arsenide has strengthened by focusing on lightweight design, flexibility and overall efficiency. The GaAs is a member of the III/V compound semiconductor family, which stands out in the global solar market due to its unmatched efficiency and open circuit voltage of 1.072V [5]. Alta Devices is a leader in high-performance flexible solar cells, which is a groundbreaking achievement, setting a new world record with a remarkable 29.1% conversion efficiency for its single-junction GaAs device [23].

This research used single junction thin film GaAs solar cells to construct a PV array, developed on the basics of a single diode practical equivalent circuit model, as shown in Figure 2.

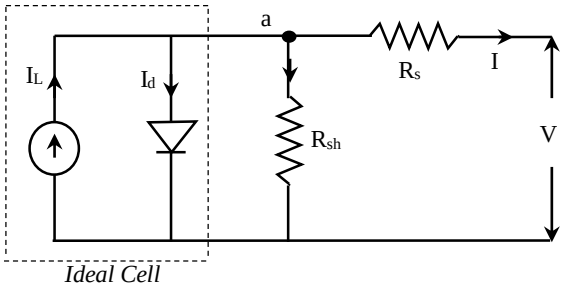

Fig. 2 General equivalent circuit model of a solar cell

Applying Kirchhoff's current law to the node 'a', the PV cell current (I) will be given in Equation 1,

$$I = I_{ph} - I_o\left(e^{\frac{q(V+I*R_S)}{nkT}} - 1\right) - \frac{V+(I*R_S)}{R_{sh}} \qquad (1)$$

The open circuit voltage of a solar cell at zero cell current is given in Equation 2,

$$V = V_{oc} = \frac{nkT}{q}\ln\left(\frac{I_L}{I_o} + 1\right) \text{ for } I_{sc} = 0 \qquad (2)$$

In this research, a PV array has been developed for the specific requirements of this work, which can generate 2024W at Maximum Power Point (MPP), as given in Table 1.

Table 1. PV array specifications

S.No.	PARAMETERS	Range
1	Open Circuit Voltage	1.072V
2	Maximum Cell Voltage	0.964V
3	Number of Cells per Module	72
4	Open Circuit Voltage/Module (V_{oc})	77.18V
5	Short Circuit Current/Module (I_{sc})	3.241A
6	Voltage at MPP/Module (V_{mpp})	69.40V
7	Current at MPP/Module (I_{mpp})	2.916A
8	Number of Parallel Strings	10
9	Number of Series Modules	1
10	Array Open Circuit Voltage (V_{oc})	77.18V
11	Array Short Circuit Current (I_{sc})	32.41A
12	Array Voltage at MPP (V_{mpp})	69.40V
13	Array Current at MPP (I_{mpp})	29.16A
14	Array Power at MPP (P_{mpp})	2024W

2.2. Enhanced DC-DC Boost Converter

The DC-DC boost converter plays a crucial role in renewable energy systems by elevating a low input voltage to a desired higher level. In this research, an optimal DC-DC boost converter is designed to address the challenges posed by unpredictable meteorological conditions. The aim is to minimize output ripples by incorporating an inductor and capacitance-based filter. The simulation model of the PV system integrated with an enhanced DC/DC boost converter and SVR model-based MPPT control is shown in Figure 3.

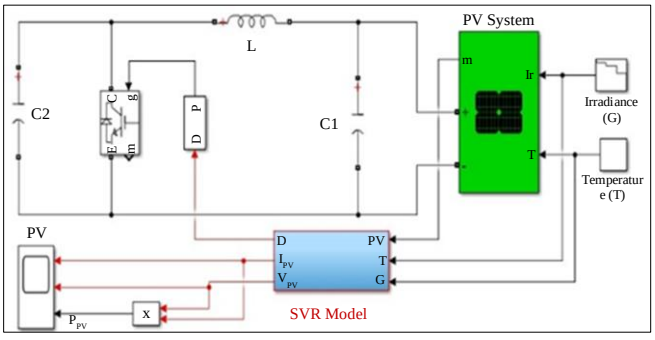

Fig. 3 Simulation model of PV array with enhanced DC/DC boost converter

The design takes into account fluctuating irradiance levels, which is ranging from a maximum of 1000 W/M^2 at Standard Test Conditions (STC) to a minimum of 50 W/M^2 (worst) with a constant temperature of 25°C. The converter is planned to efficiently adapt to these varying conditions by ensuring stable and reliable performance in renewable energy applications.

The R_{MPP} is calculated for both STC and worst conditions using the derivation 3. The converter uses a switching Frequency (F_{SW}) of 10KHZ to ensure the effective voltage transformation from the lower input level to the desired higher output level.

$$\text{Internal Resistance of PV Array } (R_{MPP}) = \frac{V_{MPP}}{I_{MPP}} \quad (3)$$

$$\text{Load Resistance } (R_O) = 2.5 \times R_{MPP} \text{ at worst} \quad (4)$$

$$\text{Duty Cycle } (D_{MPP}) \text{ at STC} = 1 - \sqrt{\frac{R_{MPP}\text{at STC}}{R_O}} \quad (5)$$

$$D_{MPP} \text{ at Worst} = 1 - \sqrt{\frac{R_{MPP} \text{ at worst}}{R_O}} \quad (6)$$

The converter output voltage (V_{OUT}) and current (I_{OUT}) are calculated for both STC and worst conditions using the Equations 7 and 8.

$$V_{OUT} \text{ at STC, Worst} = \frac{V_{IN}}{1 - D_{MPP}\text{at STC,worst}} \quad (7)$$

$$I_{OUT} \text{ at STC, Worst} = \frac{V_{OUT}\text{at STC,worst}}{R_O} \quad (8)$$

The expression 9 illustrates the impact of reflected input resistance (R_R) on the load resistance and the duty cycle. The R_R is calculated by considering the duty cycle of STC and worst conditions.

$$R_R = R_L(1 - D)^2 \quad (9)$$

The range of converter active elements was calculated using the above specific derivations in Equations 10 to 12.

$$C_1 = \frac{4V_{MPP}(STC)D_{MPP}(STC)}{\Delta V_{IN}(STC)R_R(STC)F_{SW}} \quad (10)$$

$$L = \frac{V_{MPP}(worst)D_{MPP}(worst)}{2\Delta I_{OUT}(worst)F_{SW}} \quad (11)$$

$$C_2 = \frac{2V_{OUT}(STC)D_{MPP}(STC)}{\Delta V_{OUT}(STC)R_L F_{SW}} \quad (12)$$

2.3. Bi-Directional Converter Design for Standby Battery

A standby battery system with a capacity of 40 ampere-hours (40AH), 240V (20×12) Lithium-ion (Li-ion) battery with a switching frequency of 10KHZ has been equipped with a bi-directional converter, and an auto-tuned Proportional-Integral (PI) controller represents an advanced energy storage and management solution.

Incorporating the auto-tuned PI controller enhances the efficiency and responsiveness of the bi-directional converter by ensuring optimal performance during both charging and discharging operations. The combination of the bi-directional converter operates with the dc link reference voltage of 440V, and the auto-tuned PI controller enables efficient energy routing, maximizing the performance and lifespan of the battery. The unique model of bidirectional DC/DC converter is implemented in both standby and EV batteries, which are calculated using the Equations 13, 14, 15, 16 and 17, respectively,

$$I_{outmax} = \frac{P_{PV}}{V_{out}} \quad (13)$$

$$\Delta I_L = 0.01 \times I_{outmax} \times ({}^{V_{out}}/_{V_{in}}) \quad (14)$$

$$\Delta V_{out} = 0.01 \times V_{out} \quad (15)$$

$$L = \frac{(V_{in} \times (V_{out} - V_{in}))}{(\Delta I_L \times F_{SW} \times V_{out})} = 0.1294H \quad (16)$$

$$C = \frac{(I_{outmax} \times (1 - (V_{in}/V_{out})))}{(F_{SW} \times \Delta V_{out})} = 47.5e\mu F \quad (17)$$

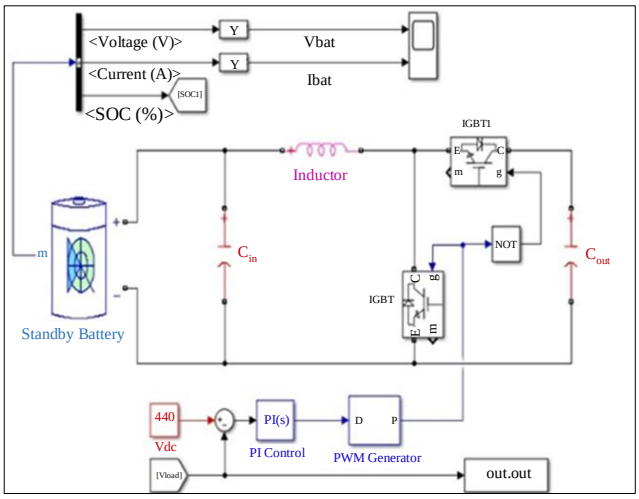

Fig. 4 Simulation model of standby battery with PI control

The role of standby battery is very crucial in this work with three distinct operating modes, high standby (>75%), moderate standby (≤50%) and low standby (<10%). These operating modes and PV system performance will decide the power routing in EV charging and AC grid. The simulation diagram of the standby battery, including the DC/DC bidirectional converter with auto-tuned PI controller, is shown in Figure 4.

2.4. EV Charging Station

The surge in Electric Vehicle adoption necessitates a robust and comprehensive charging infrastructure. EV charging stations are pivotal in supporting the growing fleet of electric vehicles, and their integration with DER systems provides a unique opportunity to optimize energy utilization and reduce dependence on traditional grid power. One of the key advantages of integrating EV charging stations with DER systems is the direct utilization of solar energy generated by PV systems.

EVs can be charged with clean and renewable energy depending on the power generated from PV panels, thereby reducing the overall environmental impact of transportation. This direct connection minimizes dependency on conventional grid power during daylight hours by aligning with the wider goal of sustainable and eco-friendly mobility.

The interaction between EV charging stations and DER systems is crucial in managing peak energy demand. Simultaneous charging activities during peak hours can strain the grid; the power can be efficiently directed to meet the dynamic charging demand with the help of intelligent energy routing. This optimises energy flow and contributes to grid stability and reliability.

When comparing Li-ion, lead-acid, Nickel-Cadmium (NiCd) and Nickel-Metal Hydride (NiMH) batteries for EV charging, several factors must be considered. The choice of a compact type of battery depends on various factors such as energy density, cost, cycle life, weight, and environmental impact.

Considering the current state of battery technology and the specific requirements for electric vehicles, Li-ion batteries are generally favoured for EV charging [24]. They offer a good balance of high energy density, relatively long cycle life and lower weight than lead-acid, nickel-cadmium and nickel-metal hydride batteries.

2.5. L-C-L Filter Design for UBI

Integrating a UBI with an L-C-L filter is crucial for efficient power conversion and grid synchronization. The UBI is employed to convert DC power generated by the PV system and stored in batteries into AC power suitable for feeding into the grid or supplying EV charging stations. Including an L-C-L filter enhances the performance of the inverter by mitigating harmonics and improving overall power quality [25].

The UBI output is directly fed to the L-C-L filter to minimize harmonic distortions and enhance power quality. The AC power (S) is 2000W, and the DC link voltage (V_{dc}) is 440V, the switching frequency FSW is 10KHZ, the peak AC voltage is 300V (V_{ac}), Fres is the resonant frequency, Fss is the sampling frequency, and the fundamental frequency (f) is 50HZ. ΔIL represents the peak-to-peak inductor current ripple in a converter. It is calculated as 0.2 times the ratio of the power to the peak AC voltage. The L-C-L filter consists of the primary inductor (L_P), secondary or AC grid side inductor (L_S) and a filter capacitance (C) integrated into the UBI system to address harmonic distortions and improve power quality. The sampling frequency is considered half of the switching frequency.

The primary inductor, secondary inductor, secondary side filter capacitance and resonant frequency were calculated by using the derivations 18, 19, 20 and 21, respectively,

$$L_P = \frac{V_{dc}}{4F_{SW}\Delta I_L} = 0.0072H \quad (18)$$

$$L_S = \frac{0.1\times V^2_{ac}}{S\times 2\pi f} - L_P = 0.0012H \quad (19)$$

$$C = \frac{0.05\times S}{V^2_{ac}\times 2\pi f} = 6.0172\mu F \quad (20)$$

$$F_{res} = \frac{1}{2\pi}\sqrt{\frac{L_P+L_S}{L_P\times L_S\times C}} = 2.0008KHZ \quad (21)$$

This filter minimizes voltage and current distortions, ensuring that the AC output meets grid standards and regulations. It also aids in reducing electromagnetic interference by enhancing the reliability and efficiency of the power conversion process. The simulation diagram for UBI with an L-C-L filter integrated with an AC grid is shown in Figure 5.

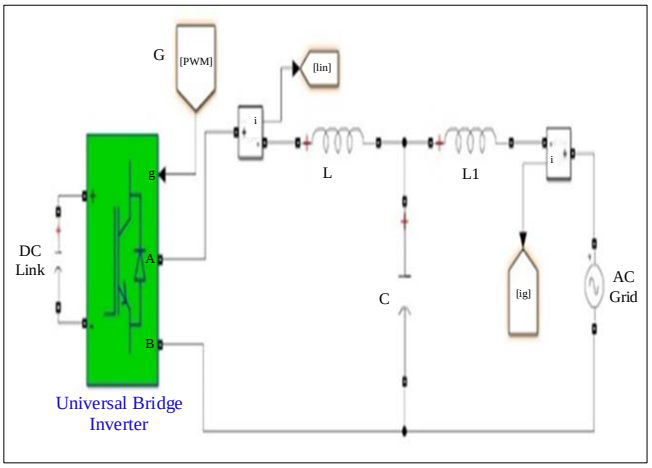

Fig. 5 UBI model with L-C-L filter integrated with AC grid

3. Control Mechanisms

3.1. ML_SVR Model for MPPT Control

ML-SVR model is highly sensible to predict the unknown parameters of PV power (P_{PV}^{MPP}) & PV voltage (V_{PV}^{MPP}) at MPP from the known data sets such as irradiance (G) & temperature (T). SVR algorithm trains (75%) and tests (25%) the input known data set and converts it to a model database to predict the unknown output parameters [26].

It is possible to improve the accuracy of fast settling time during the worst climate, reduce the error in output parameters and increase efficiency by implementing the ML-based SVR algorithm. The potential applications of SVR in MPPT lie in its capability to handle complex and non-linear relationships between input constraints (such as solar irradiance temperature) and the corresponding power output of a photovoltaic system. Traditional MPPT methods often rely on simplified models or heuristics that might not accurately capture the intricate relationships between various parameters.

The SVR-based MPPT algorithm can capture these complex relationships and provide more accurate power output forecasts. This prediction can adjust the system's operating point to maximize power, shading or partial cloud cover in rapidly changing conditions.

The SVR basic equation is formed with a training dataset with input variable 'X' and the response 'y'. The assignment of SVR is to find the regression function f(x), which predicts the y values continuously based on the input dataset X. the basic SVR equation is given in Equation 22,

$$f(x) = \sum_{i=1} N\alpha_i K(x, x_i) + b \quad (22)$$

Where, N is the number of training samples, α_i are the Lagrange multipliers associated with each training sample, x_i are the input features of the training samples, $K(x, x_i)$ is the kernel function that computes the similarity between the input features x and the training sample x_i in a transformed space, and b is the biased term. The Lagrange multipliers α_i are found by solving the dual optimization problem that involves maximizing a dual objective function subject to certain constraints, typically based on the margin and the epsilon-insensitive loss [27].

The choice of kernel function $K(x, x_i)$ depends on the problem and can be linear, polynomial, radial basis function, sigmoid, etc. The kernel function implicitly transforms the input features into a higher-dimensional space, allowing SVR to capture complex relationships between features and target values.

The P_{PV}^{MPP} always depends on the irradiance (G)and real temperature (T), and so the SVR uses G and T as input features 'x' to guess the PV voltage at maximum power point (V_{PV}^{MPP}) & PV current at maximum power point (I_{PV}^{MPP}). The predicted values of V_{PV}^{MPP} and I_{PV}^{MPP} are used to calculate Reflected input resistance (R_R), which is equal to resistance at MPP (R_{MPP})at optimized value of the DC-DC converter's duty cycle (D).

Data collection involves gathering information about the photovoltaic system's performance under various environmental conditions. This data serves as the training, testing and validation dataset for the SVR algorithm. Raw data collected from the PV system may contain noise, outliers, and irregularities affecting the SVR model's performance. Preprocessing steps are necessary to enhance data quality and model accuracy. They are data cleaning, feature selection, scaling, and data augmentation.

Support Vector Regression is a supervised learning algorithm that aims to find a function that best represents the relationship between input features and continuous output values. The key components of SVR are the Kernal function, support vectors, Epsilon-tube and regularization constant (C). The steps to implement the SVR algorithm for MPPT control in the PV system are data preparation, Kernal selection, feature scaling, parameter tuning, model training, prediction and MPPT adjustment.

Hyperparameter tuning is done to optimize the performance of the trained SVR model by adjusting the C, Epsilon and kernels. Random search or grid search methods are the methods available for this optimization. Random search is adopted in this work because it tries with all possibilities of combination. After training, the SVR model is evaluated using cross-validation, which generalizes the model to obtain unseen data.

The trained SVR model provides crucial factors to assess its performance using appropriate metrics such as Mean Squared Error (MSE), Root Mean Squared Error (RMSE) and R-squared. These metrics quantify the accuracy and reliability of the SVR predictions and their effectiveness as an MPPT controller. The workflow of the proposed ML-SVR model is shown in Figure 6.

The reflected input resistance (R_R) at MPP and duty cycle at maximum power point (D_{MPP}) is calculated as given in Equations 23 and 24, which is routed as an input for an enhanced DC/DC boost converter. The RT value is calculated using the SVR-trained model's output values (VPVMPP & IPVMPP).

$$R_T = R_{MPP} = \frac{V_{PV}^{MPP}}{I_{PV}^{MPP}} \quad (23)$$

$$D_{mpp} = 1 - \sqrt{\frac{R_T}{R_L}} \quad (24)$$

3.2. Neural Network Control for UBI

A key modernization in this research lies in applying a function-fitting neural network for precise gate pulse control of the universal bridge inverter. This neural network is an intelligent intermediary in optimizing the inverter's operation to ensure a consistent and stable grid voltage. The workflow diagram of the ANN controller model for UBI is shown in Figure 7.

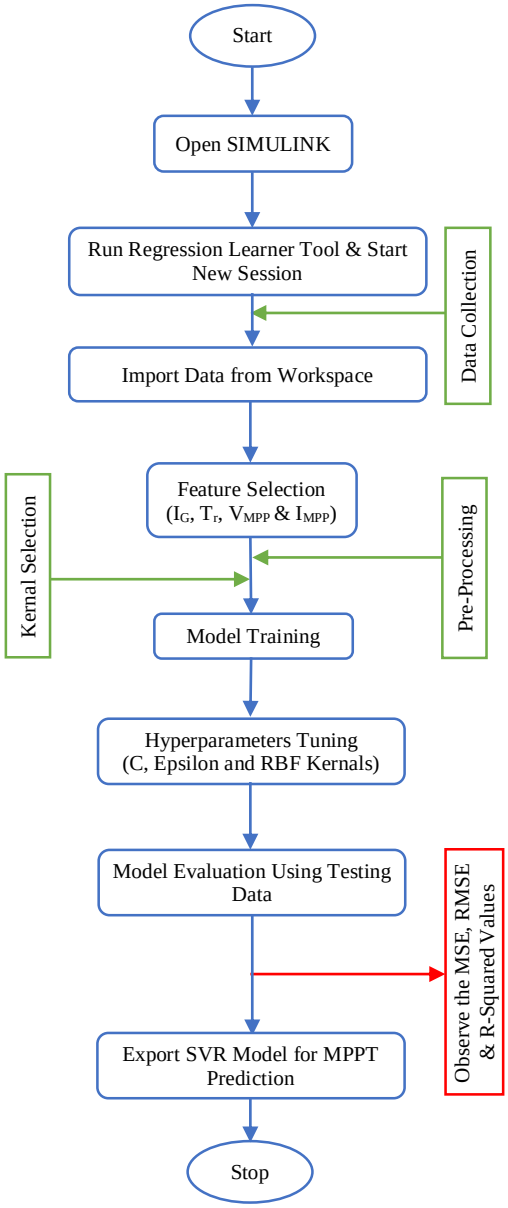

Fig. 6 ML-SVR flow chart

The neural network takes two crucial inputs: the photovoltaic power in the range of 0 to 2000W and the SOC of the standby battery in the range of 0 to 100%. The desired output is the grid voltage. Historical data on PV power and SOC of standby batteries for AC grid voltage has been collected. The obtained historical data is used to train, validate and test the function-fitting neural network.

The training process involves adjusting the weights and biases of the network to minimize the difference between the predicted grid voltage and the reference grid voltage from the training data. The difference between the expected and reference grid voltage is calculated using a loss function. The loss function quantifies the error between the predicted and actual values.

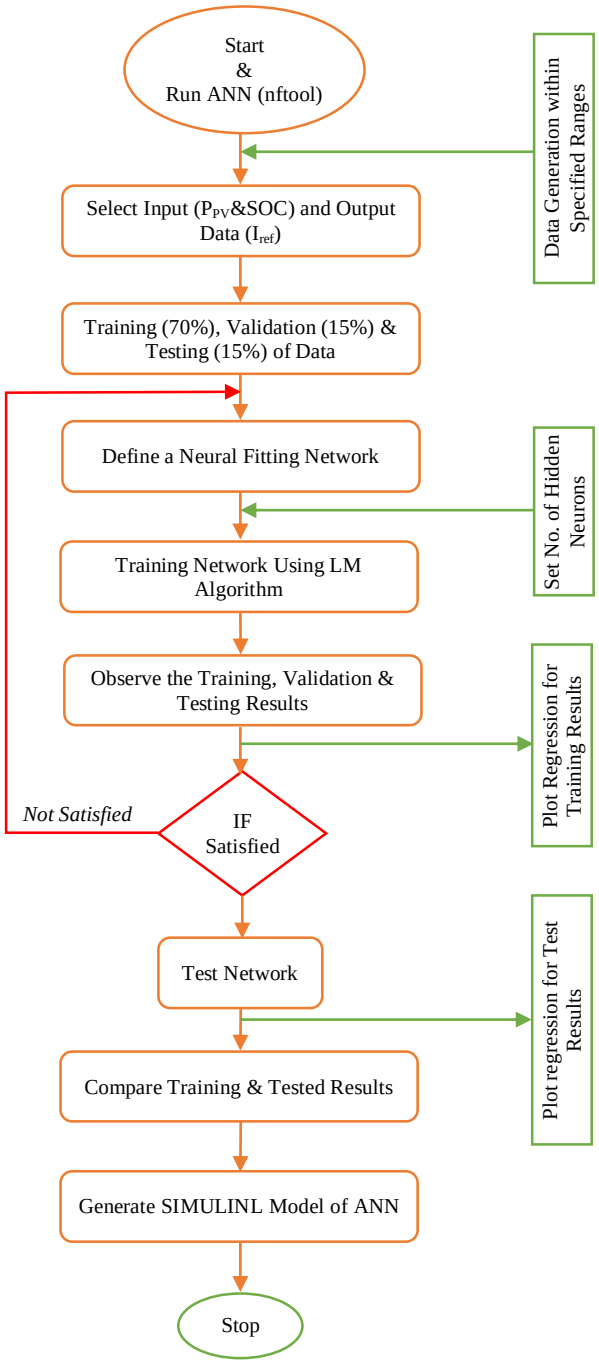

Fig. 7 Work flow of Neural Network model

The weights and biases were adjusted based on the gradient of the loss function with respect to these parameters. This step is performed using the Levenberg-Marquardt optimization method. The Levenberg-Marquardt algorithm is an optimization algorithm commonly used for solving nonlinear most minor squares problems.

The training, validation and testing data for the ANN model are shown in Figure 8. R=0.99997 indicates the predicted data is closer to or the same as the actual data.

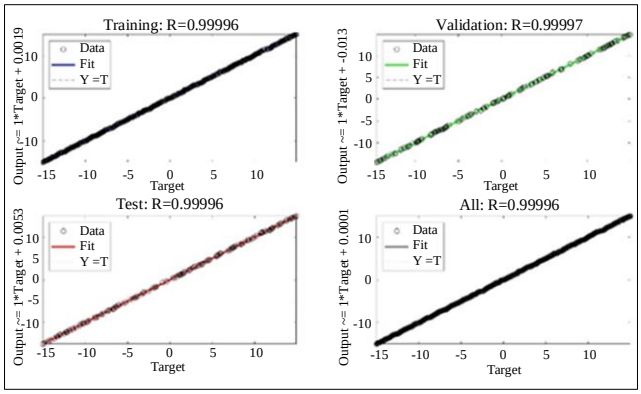

Fig. 8 R-fit comparison for trained and actual data

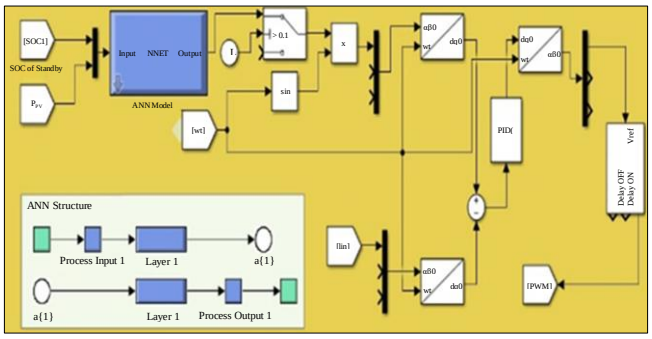

Fig. 9 Simulation diagram for ANN control mechanism for UBI

The output voltage from the neural network is then compared with the reference grid voltage of 300V AC. A comparator assesses the actual and reference voltage variance to generate an error signal that encapsulates the deviation. This error signal is a crucial metric for the subsequent control mechanisms by guiding the system towards maintaining the desired grid voltage.

The error signal from the voltage comparator is then fed into a comparison process with the inverter line current. This stage ensures synchronization between the generated voltage and the corresponding current, essential for stable grid operation. The resulting signal is then processed through a PI controller. The PI controller refines the system's response by considering both the instantaneous and cumulative errors over time.

This dual feedback mechanism enhances the system's precision and stability, ensuring an accurate correction of any deviations from the desired grid voltage. The output from the PI controller serves as the input to a Pulse Width Modulation (PWM) generator. The PWM generator converts the continuous error signal into discrete pulses by determining the duration and timing of the inverter gate pulses.

Implementing a function-fitting neural network for gate pulse control underscores a sophisticated and adaptive strategy in managing the universal bridge inverter within the DC-grid integrated PV system.

This approach not only ensures the stability of the grid voltage but also enhances the overall efficiency and responsiveness of the energy routing strategies employed in the DER system, as outlined in the earlier sections. The simulation diagram of ANN controlled mechanism for UBI is shown in Figure 9.

4. Scenarios of Operation

4.1. Higher Standby Battery SOC (>70%)

The PV system performance has been observed for different irradiance levels ranging from 1000 W/m^2 to 100 W/m^2 . The PV system consistently tracks the maximum voltage of 69V at all irradiance levels with the support of the ML-SVR model, as shown in Figure 10.

For overall analysis, DC link voltage is maintained at constant level (440V). AC grid voltage (300V) was observed with the implementation of UBI using an L-C-L filter. The DC link and AC grid voltage consistently maintain stability throughout the analysis, as shown in Figure 11.

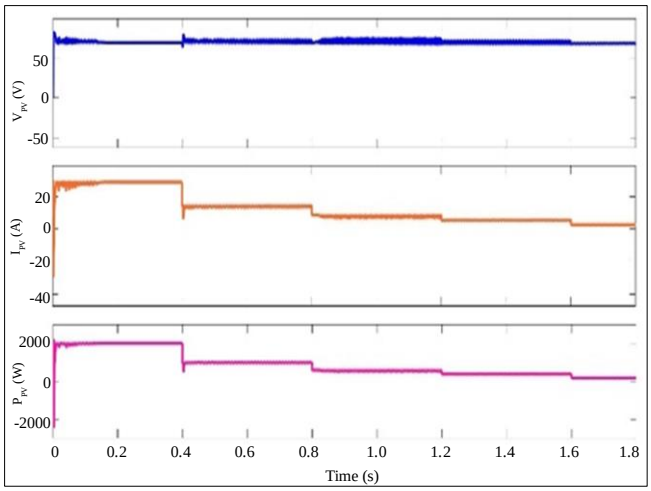

Fig. 10 PV voltage, current and power at MPP values

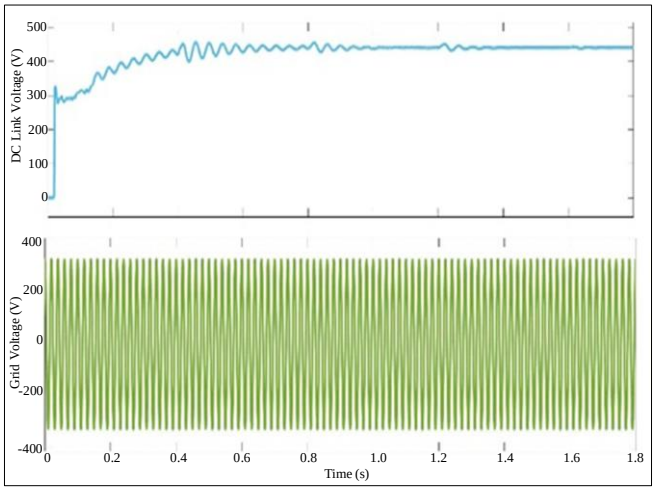

Fig. 11 DC link voltage and AC grid voltage

Both EV and standby battery voltage (240V) were maintained at stable levels throughout the analysis with the self-tuned PI controller, as shown in Figure 12. Different SOC levels (≥70%, ≤50% & <10%) were used for standby battery and EV battery SOC of 9%, as shown in Figure 13.

Including real power routing information for different SOC levels and irradiance conditions adds valuable insights into the energy distribution strategies implemented in this work. The overall system's response to different SOC levels with the interaction between the PV system, standby battery, EV battery, and AC grid has been well-documented in the discussions below.

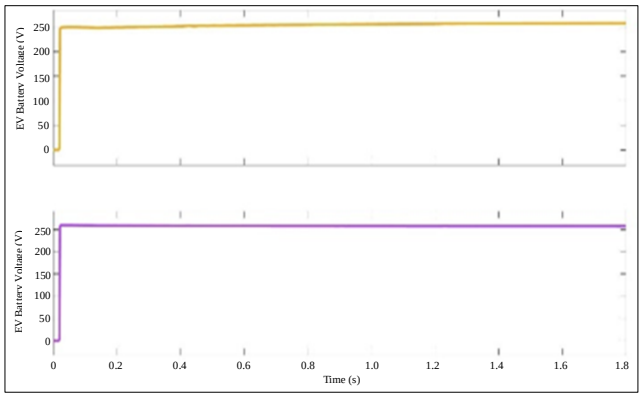

Fig. 12 EV battery voltage and standby battery voltage

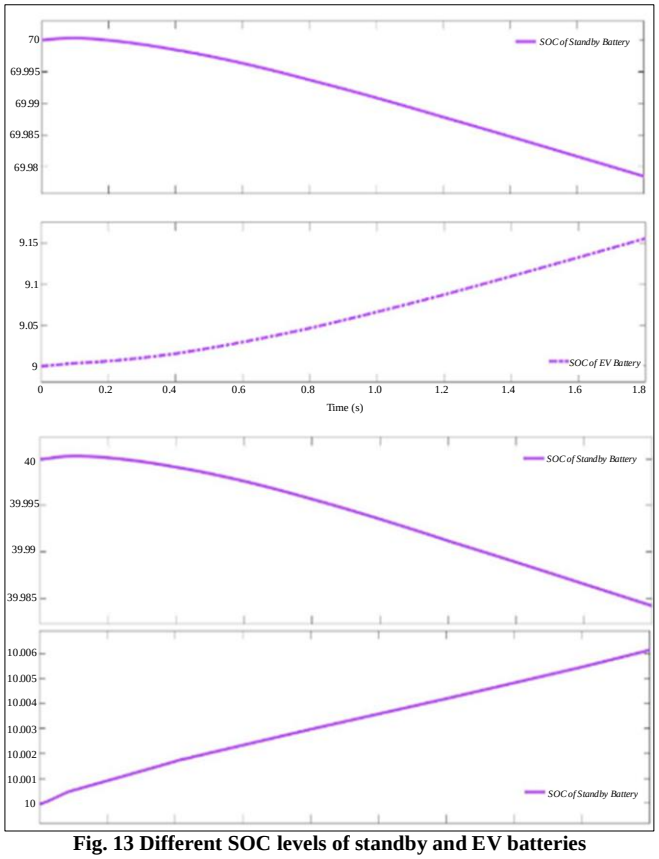

Fig. 13 Different SOC levels of standby and EV batteries

At G = 1000 W/M² (t = 0 to 0.4 sec), the PV system generated power of 2kW, and the standby battery contributes with 70% SOC, resulting in a total power injection into the grid. The generated power is also used to charge the EV battery. Both grid current and inverter currents are monitored.

At G = 500 W/M² (t = 0.4 to 0.8 sec), power injected into the grid indicates the excess energy production from the PV system and standby battery. The surplus energy is routed to the grid while charging the EV battery. Inverter and Grid currents are measured to monitor the power flow, as shown in Figure 15.

At G = 300 W/M² (t = 0.8 to 1.2 sec), the EV battery starts drawing power from the grid with decreased solar irradiance. The EV battery utilizes grid power due to the lower availability of solar energy, demonstrating the dynamic response to varying environmental conditions.

At G = 200 W/M² (t = 1.2 to 1.6 sec), the grid supplies maximum power to meet the energy demand for EV charging by compensating for the impact of reduced solar irradiance. An increase in grid currents is observed as the system relies more on grid power under challenging irradiance conditions.

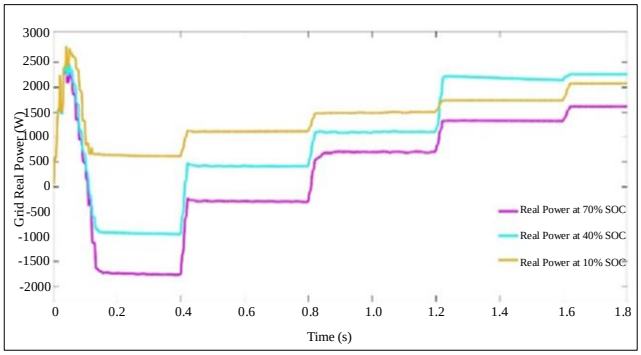

Fig. 14 AC grid power flow for different SOC levels

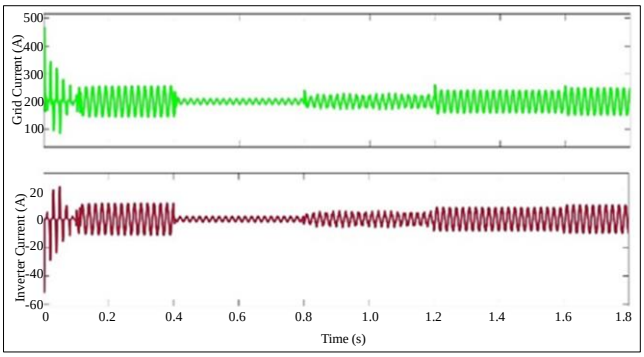

Fig. 15 Grid and Inverter currents for 70% SOC of standby battery

At G = 100 W/M² (t = 1.6 to 1.8 sec), The grid continuously provides power to sustain EV charging by adapting to the further decrease in solar irradiance. The proposed system efficiently manages energy flow to ensure

uninterrupted EV charging by emphasizing the importance of grid support during low irradiance periods. In this way, the AC grid acts as both an intake and supply source by contributing to the stability and reliability of the proposed energy system across different solar irradiance levels at different SOC levels of standby battery, as shown in Figure 14.

4.2. Moderate Standby Battery SOC (<50%)

The standby battery is in the discharging mode with a moderate SOC of 40%, indicating the active contribution to the power supply.

At G = 1000 W/M^2 (t = 0 to 0.4 sec), The PV system generates 2 kW, and the standby battery is discharging to the overall power supply. The PV system and standby battery charge the EV battery and supply power to the grid, as shown in Figure 14. Grid power is negative, which indicates the power injection into the grid.

At G = 500 W/M^2 (t = 0.4 to 0.8 sec), the AC grid intervenes early to supply power due to decreased solar irradiance and the moderate SOC of the standby battery. The EV battery receives power from the PV system, the standby battery (with a moderate SOC) and the AC grid to ensure an uninterrupted and reliable power supply.

At G = 300 W/M^2 (t = 0.8 to 1.2 sec), the AC grid's contribution to supplying real power increases with a further reduction in PV power. The EV battery utilizes power from both the grid and standby battery to compensate for the diminishing availability of solar energy. At G = 200 W/M^2 (t = 1.2 to 1.6 sec), the AC grid supplies maximum power to meet the energy requirements for EV charging under challenging irradiance conditions. Grid currents increase accordingly, as shown in Figure 16. The system adapts to the worst irradiances by relying significantly on grid power to ensure sustained charging for the EV. But the situations like worst irradiances (below 400 W/M^2) happens in the worst scenarios.

At G = 100 W/M^2 (t = 1.6 to 1.8 sec), AC grid continues to provide power to sustain EV charging during extremely low irradiance conditions. Grid currents increase as the system prioritizes grid support to meet energy demands.

4.3. Low Standby Battery SOC (<10%)

The PV system initially contributes its maximum power, and the grid provides power to charge both batteries. The EV and standby batteries are in setting mode with charging currents represented by negative values.

At G = 1000 W/M^2 (t = 0 to 0.4 sec), The PV system initially contributes its maximum power of 2 kW. The EV and standby batteries are charging by drawing power from the PV system and, at minimum, from the grid, as shown in Figure 17.

Charging currents for both batteries are negative, indicating energy absorption, as shown in Figure 18. At G = 500 W/M^2 (t = 0.4 to 1.0 sec), due to variations in irradiances, the PV system reduces its power contribution. The AC grid contributes power for EVs and standby battery charging to compensate for the reduced solar power. Charging currents for both batteries remain negative as they absorb energy from the PV system and the grid.

At G = 300 W/M^2 (t = 1.0 to 1.4 sec), PV system continues to reduce its power contribution. The AC grid further increases its power contribution for charging both batteries. Grid power becomes crucial in maintaining the charging process, especially for standby batteries with low SOC. From G = 200 W/M^2 to 100 W/M^2 (t = 1.4 to 1.8 sec & 1.8 to 2.0 sec), the grid becomes the primary source for charging both batteries with the PV system's power decrease. Negative charging currents persist for both batteries, indicating the ongoing charging process. Charging currents help improve the SOC of both batteries, especially the standby battery with its initial low SOC.

The system intelligently manages power flow to ensure continuous EVs and standby batteries charging under various conditions. The system intelligently combines power from the PV system and the grid to meet energy demands. The dynamic energy routing likely assesses the available resources and adjusts the contribution from each source to ensure optimal charging, as shown in Table 2.

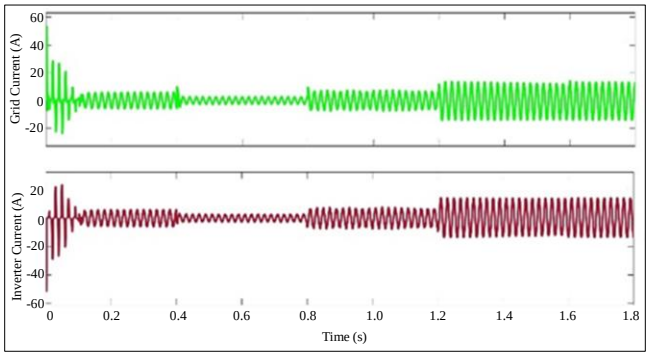

Fig. 16. Grid and inverter currents for 40% SOC of standby battery

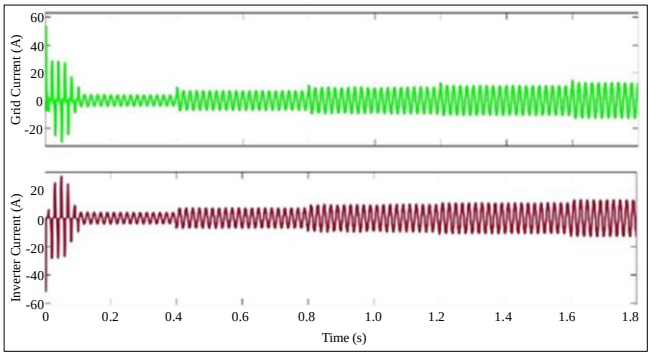

Fig. 17 Grid and inverter currents for 10% SOC of standby battery

Table 2. Contribution of grid and PV power at various conditions

SOC	1000 W/m^2		500 W/m2		300 W/m2		200 W/m2		100 W/m2	
	Grid Power	PV Power	Grid Power	PV Power	Grid Power	PV Power	Grid Power	PV Power	Grid Power	PV Power
70%	-1750w	2002w	-300w	982w	700w	530w	1325w	388w	1625w	188w
40%	-940w		-415w		1100w		2170w		2260w	
10%	620w		1113w		1490w		1740w		2078w	

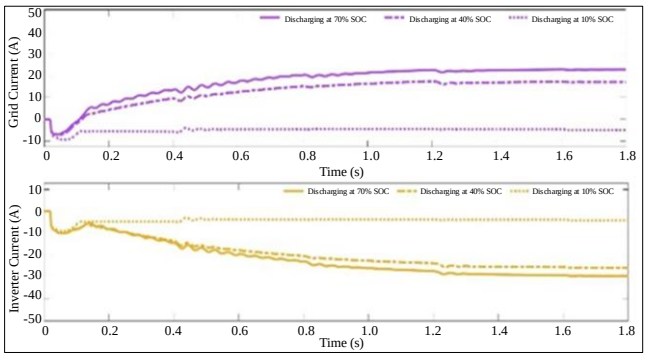

Fig. 18 Standby and EV battery currents for different SOC levels

5. Conclusion

This research presents a new approach to energy management by implementing the DER concept in a DC-grid-integrated PV system. Integrating a robust PV array with an enhanced DC-DC boost converter, an ML-SVR MPPT controller, and a standby battery synchronized with an AC grid through an ANN-controlled UBI validates a sophisticated and adaptive energy routing system.

Including an EV charging station within the DC grid further enhances the system's versatility and sustainability. The research delves into the system's dynamic behaviour under varying SOC conditions of the standby battery, proving intelligent energy routing strategies. The system efficiently manages energy flow with a higher SOC by utilizing both PV and grid power. AC grid acts as both an intake and supply source by contributing to system stability across varying solar irradiance levels.

Early intervention of the AC grid occurs with a moderate SOC to ensure adaptability to varying solar conditions. The system also adapts to low standby battery SOC by intelligently drawing power from PV and grid for charging both batteries. Dynamic adjustments ensure the efficient use of available resources to enhance the system's performance under varying solar conditions.

Grid support is dynamically managed by emphasizing its contribution to sustaining EV charging and overall system stability. The system adapts charging strategies based on SOC levels and solar irradiances. Charging currents are dynamically adjusted to show the system's ability to respond to changing energy availability.

This research contributes advanced features such as Dynamic Energy Routing, Machine Learning-based MPPT control and adaptive charging strategies based on SOC levels and solar irradiances. The findings underscore the system's ability to dynamically respond to changing energy availability, ensuring efficient use of resources and enhancing overall performance compared to more straightforward approaches outlined in the literature.

Acknowledgments

We gratefully acknowledge the support and facilities provided by the authorities of the Annamalai University, Annamalai Nagar, Tamilnadu, India, to carry out this research. We would also like to thank our supporting staff from Annamalai University, who gave insight and knowledge that considerably aided the research.

References

[1] IEA Website, Renewables 2021, IEA, Paris. [Online]. Available: https://www.iea.org/reports/renewables-2021

[2] Santosh Ghosh, and Ranjana Yadav, "Future of Photovoltaic Technologies: A Comprehensive Review," *Sustainable Energy Technologies and Assessments*, vol. 47, 2021. [CrossRef] [Google Scholar] [Publisher Link]

[3] Alexandra Catalina Lazaroiu et al., "A Comprehensive Overview of Photovoltaic Technologies and Their Efficiency for Climate Neutrality," *Sustainability*, vol. 15, no. 23, pp. 1-24, 2023. [CrossRef] [Google Scholar] [Publisher Link]

[4] Sunghyun Moon et al., "Highly Efficient Single-Junction GaAs Thin-Film Solar Cell on Flexible Substrate," *Scientific Reports*, vol. 6, pp. 1-6, 2016. [CrossRef] [Google Scholar] [Publisher Link]

[5] Martin A. Green et al., "Solar Cell Efficiency Tables (Version 60)," *Progress in Photovoltaics: Research and Applications*, vol. 30, no. 7, pp. 685-805, 2022. [CrossRef] [Google Scholar] [Publisher Link]

[6] Thai Thanh Nguyen, Hyeong-Jun Yoo, and Hak-Man Kim, "A Flywheel Energy Storage System Based on a Doubly Fed Induction Machine and Battery for Microgrid Control," *Energies*, vol. 8, no. 6, pp. 5074-5089, 2015. [CrossRef] [Google Scholar] [Publisher Link]

[7] Rohit Nishant, Mike Kennedy, and Jacqueline Corbett, "Artificial Intelligence for Sustainability: Challenges, Opportunities, and A Research Agenda," *International Journal of Information Management*, vol. 53, 2020. [CrossRef] [Google Scholar] [Publisher Link]

[8] Salman Salman, Xin AI, and Zhouyang WU, "Design of A P-&-O Algorithm Based MPPT Charge Controller for A Stand-Alone 200W PV System," *Protection and Control Modern Power Systems*, vol. 3, pp. 1-8, 2018. [CrossRef] [Google Scholar] [Publisher Link]

[9] Dezso Sera et al., "Improved MPPT Algorithms for Rapidly Changing Environmental Conditions," *12th International Power Electronics and Motion Control Conference*, Portoroz, Slovenia, pp. 1614-1619, 2006. [CrossRef] [Google Scholar] [Publisher Link]

[10] A. Frezzetti, S. Manfredi, and A. Suardi, "Adaptive FOCV-Based Control Scheme to Improve the MPP Tracking Performance: An Experimental Validation," *IFAC Proceedings Volumes*, vol. 47, no. 3, pp. 4967-4971, 2014. [CrossRef] [Google Scholar] [Publisher Link]

[11] Hegazy Rezk, and Ali M. Eltamaly, "A Comprehensive Comparison of Different MPPT Techniques for Photovoltaic Systems," *Solar Energy*, vol. 112, pp. 1-11, 2015. [CrossRef] [Google Scholar] [Publisher Link]

[12] Carlos Robles Algarín, John Taborda Giraldo, and Omar Rodríguez Álvarez, "Fuzzy Logic Based MPPT Controller for A PV System," *Energies*, vol. 10, no. 12, pp. 1-18, 2017. [CrossRef] [Google Scholar] [Publisher Link]

[13] Cesar G. Villegas-Mier et al., "Artificial Neural Networks in MPPT Algorithms for Optimization of Photovoltaic Power Systems: A Review," *Micromachines*, vol. 12, no. 10, pp. 1-19, 2021. [CrossRef] [Google Scholar] [Publisher Link]

[14] A. Kumar, M. Rizwan, and U. Nangia, "Development of ANFIS-Based Algorithm for MPPT Controller for Standalone Photovoltaic System," *International Journal of Advanced Intelligence Paradigms*, vol. 18, no. 2, pp. 247-264, 2021. [CrossRef] [Google Scholar] [Publisher Link]

[15] Mpho Sam Nkambule et al., "Comprehensive Evaluation of Machine Learning MPPT Algorithms for a PV System under Different Weather Conditions," *Journal of Electrical Engineering and Technology*, vol. 16, pp. 411-427, 2020. [CrossRef] [Google Scholar] [Publisher Link]

[16] P. Venkata Mahesh, S. Meyyappan, and Rama Koteswara Rao Alla, "Maximum Power Point Tracking Using Decision-Tree Machine-Learning Algorithm for Photovoltaic Systems," *Clean Energy*, vol. 6, no. 5, pp. 762-775, 2022. [CrossRef] [Google Scholar] [Publisher Link]

[17] Bo Zhao et al., "Operation Optimization of Standalone Microgrids Considering Lifetime Characteristics of Battery Energy Storage System," *IEEE Transactions on Sustainable Energy*, vol. 4, no. 4, pp. 934-943, 2013. [CrossRef] [Google Scholar] [Publisher Link]

[18] Muhammad Hammad Saeed et al., "A Review on Microgrids' Challenges & Perspectives," *IEEE Access*, vol. 9, pp. 166502-166517, 2021. [CrossRef] [Google Scholar] [Publisher Link]

[19] Sigma Ray et al., "Review of Electric Vehicles Integration Impacts in Distribution Networks: Placement, Charging/Discharging Strategies, Objectives and Optimisation Models," *Journal of Energy Storage*, vol. 72, Part D, 2023. [CrossRef] [Google Scholar] [Publisher Link]

[20] K.N. Nwaigwe, P. Mutabilwa, and E. Dintwa, "An Overview of Solar Power (PV Systems) Integration into Electricity Grids," *Materials Science for Energy Technologies*, vol. 2, no. 3, pp. 629-633, 2019. [CrossRef] [Google Scholar] [Publisher Link]

[21] Md. Shohag Hossain, Naruttam K. Roy, and Md. Osman Ali, "Modeling of Solar Photovoltaic System Using MATLAB/Simulink," *19th International Conference on Computer and Information Technology (ICCIT)*, Dhaka, Bangladesh, pp. 128-133, 2016. [CrossRef] [Google Scholar] [Publisher Link]

[22] Taesoo D. Lee, and Abasifreke U. Ebong, "A Review of Thin Film Solar Cell Technologies and Challenges," *Renewable and Sustainable Energy Reviews*, vol. 70, pp. 1286-1297, 2017. [CrossRef] [Google Scholar] [Publisher Link]

[23] Why Use Gallium Arsenide Solar Cells? - Alta Devices, The Atla Devices Website, 2022. [Online]. Available: https://www.altadevices.com/use-gallium-arsenide-solar-cells/

[24] Abdul Ghani Olabi et al., "Rechargeable Batteries: Technological Advancement, Challenges, Current and Emerging Applications," *Energy*, vol. 266, 2023. [CrossRef] [Google Scholar] [Publisher Link]

[25] Ignacio Villanueva et al., "L vs. LCL Filter for Photovoltaic Grid-Connected Inverter: A Reliability Study," *International Journal of Photoenergy*, vol. 2020, pp. 1-10, 2020. [CrossRef] [Google Scholar] [Publisher Link]

[26] Pradeep Kumar S., Vidhya Koothupalakkal Viswambharan, and Swaroop Pillai, "Performance Analysis of Maximum Power Point Tracking of PV Systems Using Artificial Neural Networks and Support Vector Machines," *International Conference on Computational Intelligence and Knowledge Economy (ICCIKE)*, Dubai, United Arab Emirates, pp. 511-515, 2023. [CrossRef] [Google Scholar] [Publisher Link]

[27] Chih-Chung Chang, and Chih-Jen Lin, "LIBSVM: A Library for Support Vector Machines," *ACM Transactions on Intelligent Systems and Technology*, vol. 2, no. 3, pp. 1-27, 2011. [CrossRef] [Google Scholar] [Publisher Link]

[28] Dominic Savio Abraham et al., "Fuzzy-Based Efficient Control of DC Microgrid Configuration for PV-Energized EV Charging Station," *Energies*, vol. 16, no. 6, pp. 1-17, 2023. [CrossRef] [Google Scholar] [Publisher Link]

[29] Youssef Alidrissi et al., "An Energy Management Strategy for DC Microgrids with PV/Battery Systems," *Journal of Electrical Engineering & Technology*, vol. 16, pp. 1285-1296, 2021. [CrossRef] [Google Scholar] [Publisher Link]